Article:
Liao, X., Fan, L., Wang, Y. et al. (2023) Attenuation characterization of terahertz waves in foggy and rainy conditions at 0.1–1 THz frequencies. Electronics, 12 (7). 1684. ISSN: 1450-5843

https://doi.org/10.3390/electronics12071684

electronics

MDPI

Article

Attenuation Characterization of Terahertz Waves in Foggy and Rainy Conditions at 0.1–1 THz Frequencies

Xi Liao [1,2], Linjie Fan [1,2], Yang Wang [1,2,*], Ziming Yu [3,†], Guangjian Wang [3,†], Xianjin Li [3,†] and Jie Zhang [4,†]

[1] School of Communication and Information Engineering, Chongqing University of Posts and Telecommunications, Chongqing 400065, China; liaoxi@cqupt.edu.cn (X.L.)
[2] Chongqing Key Laboratory of Complex Environmental Communications, Chongqing 400065, China
[3] Huawei Technologies Co., Ltd., Chengdu 611730, China
[4] Department of Electronic and Electrical Engineering, The University of Sheffield, Sheffield S10 2TN, UK
* Correspondence: wangyang@cqupt.edu.cn
† These authors contributed equally to this work.

Abstract: Investigating the absorption and scattering effects of atmospheric particles, i.e., raindrops and fog droplets, is required to establish a comprehensive and accurate channel model. However, for long-distance communication in outdoor scenarios, research on the propagation characterization of fog and rain attenuation in the terahertz (THz) band is insufficient. In this study, fog and rain attenuation characterization with different conditions are characterized. First, fog attenuation at different temperatures and diverse visibility is explored using Rayleigh approximation theory and Mie theory. The results demonstrate that visibility and frequency have a stronger effect than temperature on fog attenuation. Then, rain attenuation as a function of rainfall rate is theoretically determined using Mie theory and the Joss, M-P, and Weibull distribution. The results show that rainfall rate and frequency have greater impact than raindrop distribution on rain attenuation. There are large differences in rainfall attenuation under diverse distributions. Accurate fog and rainfall attenuation information can be used to better estimate path loss and the link budget for terahertz communication in outdoor scenarios.

Keywords: 6G; THz communication; fog and rain attenuation; Rayleigh approximation theory; Mie theory

Citation: Liao, X.; Fan, L.; Wang, Y.; Yu, Z.; Wang, G.; Li, X.; Zhang, J. Attenuation Characterization of Terahertz Waves in Foggy and Rainy Conditions at 0.1–1 THz Frequencies. *Electronics* **2023**, *12*, 1684. https://doi.org/10.3390/electronics12071684

Academic Editor: Christos J. Bouras

Received: 13 March 2023
Revised: 29 March 2023
Accepted: 31 March 2023
Published: 3 April 2023

1. Introduction

To meet the growing demands for wireless communication in the real world, forthcoming wireless communication systems will require higher data rates, increased carrier frequency, and greater system capacity and bandwidth [1]. After the fifth-generation (5G) wireless communication system adopted millimeter-wave (mmWave) bands, the sixth-generation (6G) wireless communication systema are working toward adopting the terahertz (THz) band (0.1–10 THz), which offers abundant spectrum resources, being situated between microwaves and optical waves [2]. Terahertz communication is a technology that takes the terahertz band as a carrier to realize wireless communication. It is characterized by a high transmission rate, extensive capacity, and large bandwidth, which position terahertz communication technology as one of the vital technologies for the development of 6G [3–5]. Terahertz communication technology is expected to be applied in high-precision positioning, three-dimensional perception imaging, holographic communication, micro-sized communication, ultra-large-capacity data backhaul, and short-distance ultra-high-speed transmission [6–11].

Terahertz waves have a higher frequency and experience more significant path loss than millimeter waves. Additionally, terahertz waves are prone to blockage by buildings and objects and can be easily absorbed and scattered by atmospheric molecules during transmission, which leads to signal attenuation. In addition to the atmosphere, the terahertz

signal is affected by weather, such as rain and fog [12,13]. The large-sized raindrops and fog droplets on rainy and foggy days can strongly absorb and scatter terahertz waves and thus cause more significant signal attenuation. Moreover, due to the increase in the frequency band, weather conditions have increasing influences on terahertz waves. Hence, conducting intensive research on the propagation characterization of terahertz waves in atmospheric particles such as fog droplets and raindrops is crucial.

In recent years, the propagation characterization of terahertz waves in the atmosphere and under diverse weather conditions has been extensively investigated. Regarding atmospheric attenuation, in [14,15], the authors studied the influence of the atmosphere on terahertz waves, analyzed the feasibility of outdoor terahertz communication systems, and demonstrated the potential of line-of-sight terahertz communication, sensing, and imaging. Regarding fog attenuation, in [16], the transmission rate of terahertz wireless links in the frequency range of 300–900 GHz in sunny, foggy, and rainy days was investigated. In the transmission windows of 300–376 GHz and 376–434 GHz, even under the worst rainy days with a rainfall intensity of 50 mm/h, the upper limit of the data rate surpassed 10 Gbps (per 1 GHz channel bandwidth). Researchers [17] considered the attenuation of terahertz waves caused by different particles, such as fog droplets, haze particles, and raindrops, where the optical parameters of these particles were given by the analysis of meteorological data, and the scattering characteristics of THz waves were explored. In addition, it was observed that the factors, including visibility and rainfall rate, had a significant impact on the scattering characteristics of terahertz waves. In [13,18–20], propagation characteristics were investigated through theory and experimentation with terahertz waves in fog. The authors of [19,20] conducted fog attenuation experiments using a controllable fog testing chamber, in which the attenuation of terahertz waves was analyzed based on the millimeter-wave propagation model (MPM), Rayleigh approximation [21,22], and Mie theory. Furthermore, the experimental results were consistent with the model predictions, and the increase in attenuation with the decrease in the optical visibility conformed to the predicted values.

As for rain attenuation, authors [23,24] developed free-space communication channels at 625 GHz and 1550 nm and designed a controllable rainfall weather simulation room; the performance of the two channels was analyzed by measuring the power and bit error rate of each link using a terahertz time-domain spectroscopy system. Given the results, the attenuation of terahertz and the infrared waves was comparable in typical rain conditions. In addition, in [25,26], the rain attenuation of THz waves was estimated by collecting local rainfall data based on Mie theory, which was compared with the results of the International Telecommunication Union Radiocommunication Sector (ITU-R) model. The main difference was that the former uses rainfall rate data, while the latter uses raindrop size distribution data. The authors of [25] indicated that for rainfall events greater than 10 mm/h, the average attenuation was between 8 dB/km and 18 dB/km, and the results in [26] demonstrated that the rainfall attenuation in Indonesia was smaller than that in the ITU-R model at lower frequencies, while it is larger than the ITU-R model at higher frequencies. The rain attenuation of terahertz waves at 77 GHz and 300 GHz under varying rainfall rates was investigated [27], and a series of measurements were conducted, including attenuation, rainfall rate, and droplet size distribution. In addition, the measured droplet size distribution was later compared with that obtained with commonly used models, such as the Marshall and Palmer (M-P) distribution model and Weibull distribution model, and it was concluded that the Weibull distribution model was more in line with the measured droplet size distribution.

Overall, rain and fog attenuation of terahertz waves have been widely investigated by scholars and institutions. Nevertheless, research on the systematic and comprehensive propagation characterization of rain and fog attenuation of terahertz waves is lacking, and there is a need to enhance the numerical simulation of attenuation under various conditions. To address these issues, we aimed to comprehensively characterize the propagation of rain and fog attenuation of terahertz waves. The main contributions of this work are as follows:

- In terms of fog attenuation, based on Rayleigh approximation theory and Mie theory, we investigated the influence of advection fog and radiation fog on terahertz waves and determined the attenuation in fog at diverse temperatures and visibility at 0.1–1 THz. In addition, we used a more accurate Rayleigh approximation theory and compared it with the results obtained with a reference [18].
- In terms of rain attenuation, the rain was divided into four types: drizzle, moderate rain, downpour, and rainstorm, based on the rainfall rate, and we comprehensively compared and analyzed the rain attenuation of terahertz waves under Joss, M-P, and Weibull distributions.
- The results indicate that visibility and frequency have a more significant effect than temperature on fog attenuation. The differences at 1 THz between the attenuation caused by advection fog and radiation fog are 8461.31 dB, 1986.81 dB, 250.82 dB, and 24.98 dB, corresponding to visibility of 30 m, 50 m, 100 m, and 200 m, respectively. Additionally, rainfall rate and frequency have a greater impact than raindrop distribution on rain attenuation. The rainfall attenuation significantly varies under different distributions, with the maximum difference being 3256.35 dB and the minimum difference being 0.34 dB at 1 THz.

The remainder of this paper is structured as follows: In Section 2, the propagation mechanism of terahertz waves and the distribution spectrum of fog droplets and raindrops are discussed. Section 3 presents Mie theory and Rayleigh approximation theory. Section 4 focuses on the analysis of fog and rain attenuation of terahertz waves. In Section 5, the main conclusions of this study are drawn.

2. Propagation Mechanism and Particle Distribution

To investigate terahertz wave propagation characteristics in rain and fog, it is essential to have an understanding of the electromagnetic wave propagation mechanisms and the physical characteristics of fog and raindrops since these factors are key in affecting terahertz wave attenuation. Moreover, when terahertz waves interact with fog and raindrop particles, these particles scatter and absorb the waves. The particle distribution spectrum, which describes the number of particles of various sizes, aids in accurately calculating terahertz wave attenuation. Therefore, this section first presents the propagation mechanism of electromagnetic waves and the physical characteristics of fog droplets and raindrops. Subsequently, the distribution spectra of fog droplets and raindrops are summarized.

2.1. Propagation Mechanism

The scattering of electromagnetic waves is related to heterogeneity, such as the heterogeneity at the molecular scale and the aggregation of multiple molecules. Regardless of the type of heterogeneity, the basic physics of scattering is the same for all systems. As shown in Figure 1, if an obstacle, such as a single electron, atom, molecule, or solid or liquid particles, is irradiated by electromagnetic waves, the electric field of the incident wave causes the charge in the obstacles to oscillate. It can accelerate the charges to radiate electromagnetic energy in all directions. This secondary radiation is called the radiation of obstacle scattering, which means that the scattering equals excitation plus reradiation. In addition to reradiating the electromagnetic energy, the stimulated base charges can convert part of the incident electromagnetic energy into other forms, such as thermal energy, which is called absorption [28].

2.2. Fog Droplet Distribution

The fog is a weather phenomenon where tiny droplets or ice crystals are suspended in the near-ground air, which is the product of the condensation of water vapor in the air near the ground. According to the conditions of formation, fog can be divided into advection fog and radiation fog. Advection fog is formed by the cooling of warm and moist air as it moves to cooler land or over the colder surface of water. It generally appears in areas near the sea, with a wide range and high concentration. Radiation fog is the countless small

droplets formed by the cooling of the radiation on the ground at night. It mostly occurs at night and early morning when the weather is clear, the water vapor near the surface is sufficient and stable, or there is a temperature inversion.

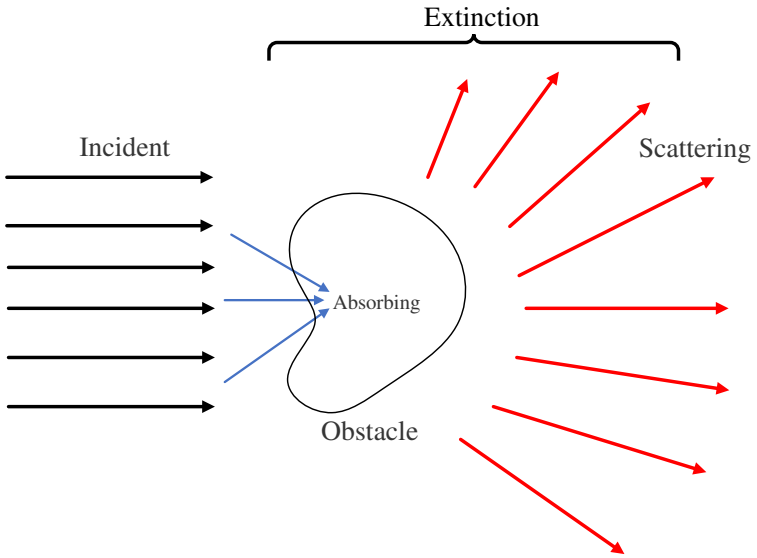

Figure 1. Obstacle absorption and scattering of incident waves.

Attenuation of terahertz waves in fog is caused by the absorption and scattering of waves by particles. The radius of these particles typically ranges between 1 μm and 60 μm. Table 1 presents the levels of fog and their corresponding horizontal visibilities (V).

Table 1. Relationship between fog level and horizontal visibility.

Fog Level	**0**	**1**	**2**	**3**	**4**	**5**
Horizontal Visibility (km)	>10	1–10	0.5–1	0.2–0.5	0.05–0.2	<0.05
Designation	Clear day	Mist	Fog	Heavy fog	Dense fog	Strong fog

The size and distribution of fog droplets can have a significant impact on terahertz wave attenuation based on Mie theory. The generalized gamma distribution is the most commonly used empirical model for describing fog droplet distribution, which is reported as [29]:

$$n(r) = ar^{\alpha} \exp(-br^{\beta}), \tag{1}$$

where r is the radius of droplet particles, and n is the number of droplets per unit volume. If the droplet radius is in microns (μm), the unit of n is $\mathrm{m}^{-3}\mu\mathrm{m}^{-1}$; if the droplet radius is in meters (m), then n is in m^{-4}. Other parameters a ($a = \frac{9.781}{V^6 M^5} \times 10^{15}$) and b ($b = \frac{1.304}{VM} \times 10^4$), describing droplet size and shape, are determined by visibility and water content; V is the fog visibility in kilometers; and M is the water content of the fog in grams per meter cumbed. When $\alpha = 2$ and $\beta = 1$, the gamma distribution can accurately describe the particle size distribution:

$$n(r) = ar^2 \exp(-br). \tag{2}$$

To calculate the density of liquid water M ($\mathrm{g/m}^3$) in advection fog and radiation fog, an empirical expression based on the fog visibility can be represented [17]:

$$\begin{cases} M = (18.35V)^{-1.43} = 0.0156V^{-1.43}, & \text{Advection fog,} \\ M = (42V)^{-1.54} = 0.00316V^{-1.54}, & \text{Radiation fog.} \end{cases} \tag{3}$$

Combining Equations (2) and (3), it can be found that:

$$\begin{cases} n(r) = 1.059 \cdot 10^7 V^{1.15} r^2 \cdot \exp(-0.8359 \cdot V^{0.43} r)(\mathrm{m}^{-3}\mu\mathrm{m}^{-1}), & \text{Advection fog,} \\ n(r) = 3.104 \cdot 10^{10} V^{1.7} r^2 \cdot \exp(-4.122 \cdot V^{0.54} r)(\mathrm{m}^{-3}\mu\mathrm{m}^{-1}), & \text{Radiation fog.} \end{cases} \quad (4)$$

2.3. Raindrop Distribution

Rain is a precipitation phenomenon where liquid droplets fall from the atmosphere to the ground. There are different types of rain, such as drizzle, continuous rain, and downpour, with raindrop radius typically ranging from 0.01 mm to 4 mm. According to meteorological standards, drizzle is defined as rainfall less than 2.5 mm/h, moderate rain ranges from 2.6 to 8.0 mm/h, downpours range from 8.1 to 15.9 mm/h, and a rainstorm is characterized by more than 16.0 mm of rainfall per hour. The attenuation of terahertz waves caused by rainfall is primarily determined by the extinction cross-section and the size distribution of raindrops. Rain attenuation can be calculated based on the size distribution of raindrop particles and Mie theory. The size distribution of raindrop particles refers to the number of raindrop particles of various sizes in rainfall, and several distribution models are commonly used, such as Joss distribution [30], M-P distribution [31], and Weibull distribution [32].

In Joss's experiment, the rainfall was classified into three categories based on intensity: drizzle with $R \leq 5$ mm/h, widespread with 5 mm/h $< R \leq 25$ mm/h, and thunderstorm with $R > 25$ mm/h. Furthermore, each type of rainfall has a specific raindrop distribution with diverse coefficients. The Joss distribution is reported as:

$$\begin{cases} \text{Drizzle} : n(r) = 30{,}000 \exp(-11.4 R^{-0.21} r), \\ \text{Widespread} : n(r) = 7000 \exp(-8.2 R^{-0.21} r), \\ \text{Thunderstorm} : n(r) = 1400 \exp(-6.0 R^{-0.21} r), \end{cases} \quad (5)$$

where R is the rainfall rate in millimeters per hour, and *r is the radius* in millimeters.

The M-P distribution was proposed by Marshall and Palmer based on measured data and is expressed as:

$$n(r) = 8000 \exp(-8.2 R^{-0.21} r)\ \mathrm{m}^{-3}\mathrm{mm}^{-1}. \quad (6)$$

In order to improve the accuracy of raindrop size distribution estimation, Jiang et al. proposed a new Weibull distribution by calculating the raindrop distribution parameters through rainfall observation experiments, which is represented as:

$$n(r) = N_0 \frac{\eta}{\sigma} \left(\frac{2r}{\sigma}\right)^{\eta-1} \exp\left[-\left(\frac{2r}{\sigma}\right)^{\eta}\right], \quad (7)$$

where $N_0 = 1000\ \mathrm{m}^{-3}$, $\eta = 0.95 R^{-3}$, $\sigma = 0.26 R^{0.42}$.

3. Theoretical Model

In order to precisely calculate fog and rain attenuation, rational mathematical models are required. This section presents Rayleigh approximation theory and Mie theory, which were adopted in this study. The detailed calculation methods of the related parameters, including the attenuation coefficient, extinction efficiency factor, and scattering coefficient, are provided. Additionally, the dominant extinction efficiency factor in Mie theory is simulated and analyzed.

3.1. Rayleigh Approximation Theory

Given the relatively small radius of fog droplets, the Rayleigh approximation model is suitable for calculating fog attenuation. In accordance with this model, the fog attenuation of terahertz waves can be expressed as [33]:

$$\alpha_c = K_f \cdot M \ (\mathrm{dB/km}), \tag{8}$$

where M is the density of liquid water in fog (g/m^3); K_f is the attenuation coefficient in ((dB/km)/(g/m^3)), which is calculated by:

$$\begin{cases} K_f = \frac{0.819f}{\varepsilon''(1+\eta^2)}, \\ \eta = \frac{2+\varepsilon'}{\varepsilon''}, \end{cases} \tag{9}$$

where f is the signal frequency (GHz); ε' and ε'' are the real and imaginary parts of the complex permittivity, respectively, which are determined by:

$$\begin{cases} \varepsilon'(f) = \frac{\varepsilon_0-\varepsilon_1}{\left[1+(f/f_p)^2\right]} + \frac{\varepsilon_1-\varepsilon_2}{\left[1+(f/f_s)^2\right]} + \varepsilon_2, \\ \varepsilon''(f) = \frac{(\varepsilon_0-\varepsilon_1)f}{f_p\left[1+(f/f_p)^2\right]} + \frac{(\varepsilon_1-\varepsilon_2)f}{f_s\left[1+(f/f_s)^2\right]}, \end{cases} \tag{10}$$

where $\varepsilon_0 = 77.66 + 103.3(\theta - 1)$, $\varepsilon_1 = 0.0671\varepsilon_0$, $\varepsilon_2 = 3.52$, $\theta = 300/(273.15 + T)$, and T is the temperature of rain and fog (°C).

The main relaxation frequency f_p and the secondary relaxation frequency f_s are:

$$\begin{cases} f_p = 20.20 - 146(\theta - 1) + 316(\theta - 1)^2 \ \ (\mathrm{GHz}), \\ f_s = 39.8 f_p \ \ (\mathrm{GHz}). \end{cases} \tag{11}$$

3.2. Mie Theory

Compared with the Rayleigh approximation, Mie theory, proposed by Gustav Mile in 1908, was deduced based on the solution of the Maxwell equations. It assumes particles are ideal spheres and adopts the spherical Bessel function to obtain related parameters. The main objective of Mie theory is to address the issue of absorption and scattering of light by spherical particles. Despite its limitations, Mie theory can accurately describe the effects of small particles that are not immediately apparent. According to Mie theory, particle attenuation is primarily characterized by the extinction cross-section, scattering cross-section, and absorption cross-section, which can be separately expressed as [28]:

$$\begin{cases} C_e(r,\lambda,m) = \frac{\lambda^2}{2\pi} \sum\limits_{n=1}^{\infty} (2n+1)\mathrm{Re}(a_n + b_n), \\ C_s(r,\lambda,m) = \frac{\lambda^2}{2\pi} \sum\limits_{n=1}^{\infty} (2n+1)\left(|a_n|^2 + |b_n|^2\right), \\ C_a(r,\lambda,m) = C_e(r,\lambda,m) - C_s(r,\lambda,m). \end{cases} \tag{12}$$

The efficiency factors for the extinction, scattering, and absorption are defined as:

$$\begin{cases} Q_e(r,\lambda,m) = \frac{C_e(r,\lambda,m)}{\pi r^2}, \\ Q_s(r,\lambda,m) = \frac{C_s(r,\lambda,m)}{\pi r^2}, \\ Q_a(r,\lambda,m) = \frac{C_a(r,\lambda,m)}{\pi r^2}. \end{cases} \tag{13}$$

Therefore, it is evident that:

$$\begin{cases} Q_e(x,m) = \frac{2}{x^2}\sum\limits_{n=1}^{\infty}(2n+1)\mathrm{Re}(a_n+b_n), \\ Q_s(x,m) = \frac{2}{x^2}\sum\limits_{n=1}^{\infty}(2n+1)\left(|a_n|^2+|b_n|^2\right), \\ Q_a(x,m) = Q_e(x,m) - Q_s(x,m), \end{cases} \tag{14}$$

where m is the refractive index of the particle relative to the surrounding medium, $m = m_1 + m_2$. As for the size parameter of the particles, $x = kr$, and $k = 2\pi/\lambda$. r is the radius of the particle, and λ is the length of the incident waves.

If the scattering coefficients a_n and b_n are known, all measurable quantities related to scattering and absorption, such as cross-sections and scattering matrix elements, can be determined. By applying boundary conditions for magnetic and electric fields, expanding the incident, internal, and scattered magnetic fields into series, and using expressions for vector harmonics, a set of linear equations is established, from which the scattering coefficients a_n and b_n can be calculated [28]:

$$a_n = \frac{\psi'_n(mx)\psi_n(x) - m\psi_n(mx)\psi'_n(x)}{\psi'_n(mx)\xi_n(x) - m\psi_n(mx)\xi'_n(x)}, \tag{15}$$

$$b_n = \frac{m\psi'_n(mx)\psi_n(x) - \psi_n(mx)\psi'_n(x)}{m\psi'_n(mx)\xi_n(x) - \psi_n(mx)\xi'_n(x)}, \tag{16}$$

where $\psi_n(x)$ and $\xi_n(x)$ are the n-order spherical Bessel functions of the first kind and the first type of the n-order spherical Bessel functions of the third kind, respectively. $\psi'_n(x)$ and $\xi'_n(x)$ are the derivatives of $\psi_n(x)$ and $\xi_n(x)$, respectively. The n-order spherical Bessel functions of the first kind and the third kind are calculated as:

$$\psi_n(x) = xj_n(x) = \sqrt{\frac{\pi x}{2}}J_{n+0.5}(x) \tag{17}$$

$$\xi_n(x) = xh_n^{(1)}(x) = \sqrt{\frac{\pi x}{2}}H_{n+0.5}^{(1)}(x) \tag{18}$$

where x is the size parameter of the particle, determined by the particle radius and the wavelength of the incident wave; $J_{n+0.5}(x)$ is a Bessel function of the first kind of half-integer order; and $H_{n+0.5}^{(1)}(x)$ is a Bessel function of the first one of the third kind of the half-integer order. Functions $j_n(z)$ and $h_n^{(1)}(z) = j_n(z) + iy_n(z)$ are the spherical Bessel functions ($z = x$ or mx) of order n ($n = 1, 2, \ldots$). The derivative of the spherical Bessel function is represented as [34]:

$$\begin{cases} [zj_n(z)]' = zj_{n-1}(z) - nj_n(z), \\ \left[zh_n^{(1)}(z)\right]' = h_{n-1}^{(1)}(z) - nh_n^{(1)}(z). \end{cases} \tag{19}$$

For integrity, the relationship between the Bessel function and the spherical Bessel function is reported as:

$$\begin{cases} j_n(z) = \sqrt{\frac{\pi}{2z}}J_{n+0.5}(z), \\ y_n(z) = \sqrt{\frac{\pi}{2z}}Y_{n+0.5}(z), \end{cases} \tag{20}$$

where $J_n(z)$ and $Y_n(z)$ are the Bessel functions of the first and second kinds, respectively. When n = 0 and 1, the spherical Bessel function can be given by:

$$\begin{cases} j_0(z) = \frac{\sin z}{z}, \\ j_1(z) = \frac{\sin z}{z^2} - \frac{\cos z}{z}, \\ y_0(z) = -\frac{\cos z}{z}, \\ y_1(z) = -\frac{\cos z}{z^2} - \frac{\sin z}{z}. \end{cases} \tag{21}$$

In addition, the recursive formula is defined as:

$$f_{n-1}(z) + f_{n+1}(z) = \frac{2n+1}{z} f_n(z), \tag{22}$$

where $f_n(z)$ can be any one of the function $j_n(z)$ and function $y_n(z)$.

As shown in Figure 2, the extinction efficiency factor oscillates with increasing size parameter, significantly oscillating within the range of 0 to 20. In the range of 20 to 60, the extinction efficiency factor tends to gradually stabized, and its value is stable at about 2.1. The figure shows a series of broader maxima and minima that manifest the interference between incident light and forward scattered light. Energy conservation requires that the light scattered in all directions and absorbed in particles is equivalent to the light eliminated by the interference from the incident beam.

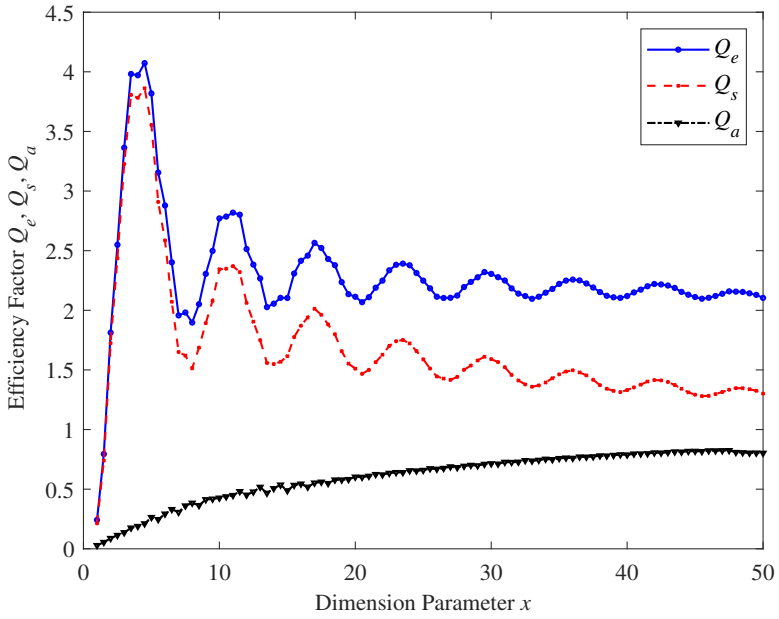

Figure 2. Relationship between dimension parameter x and efficiency factor.

When the particle distribution spectrum is known, the particle attenuation of terahertz waves can be calculated by integrating the radii of all particles [25]:

$$\begin{aligned} A &= 4.343 \times 10^3 \int_{r_{\min}}^{r_{\max}} Q_e(r, \lambda, m) \cdot \pi r^2 \cdot n(r) dr \\ &= 4.343 \times 10^3 \int_{r_{\min}}^{r_{\max}} C_e(r, \lambda, m) \cdot n(r) dr (\mathrm{dB/km}). \end{aligned} \tag{23}$$

4. Results and Analysis

To comprehensively investigate the attenuation of terahertz waves in fog and rain, this section first compares and analyzes the impact of radiation and advection fog on terahertz wave attenuation for diverse temperatures and visibility conditions and compares the findings with those of [18]. Secondly, fog attenuation under different visibility conditions is analyzed based on Mie theory. Finally, an analysis of rain attenuation in terms of frequency, rainfall rate, and raindrop distribution is presented.

4.1. Fog Attenuation Based on the Rayleigh Approximation

Letting V = 30 m, the radiation and advection fog attenuation under different temperatures are shown in Figure 3. At first, fog attenuation gradually increases with an increase in frequency. Second, radiation fog attenuation is significantly less than advection fog attenuation. For instance, in area II (0.24–1 THz), when the temperature is 30 °C and the frequency is increased from 0.25 THz to 1 THz, the difference between the two types of fog attenuation increases from 22.16 dB/km to 71.34 dB/km. Third, the fog attenuation of terahertz waves hardly changes in area I (0.1–0.24 THz). However, fog attenuation increases with temperature in area II, but the upward trend gradually reduces. Therefore, the temperature significantly affects fog attenuation in the high-frequency band of terahertz waves. In contrast, the temperature has little impact on fog attenuation in the low-frequency band of terahertz waves.

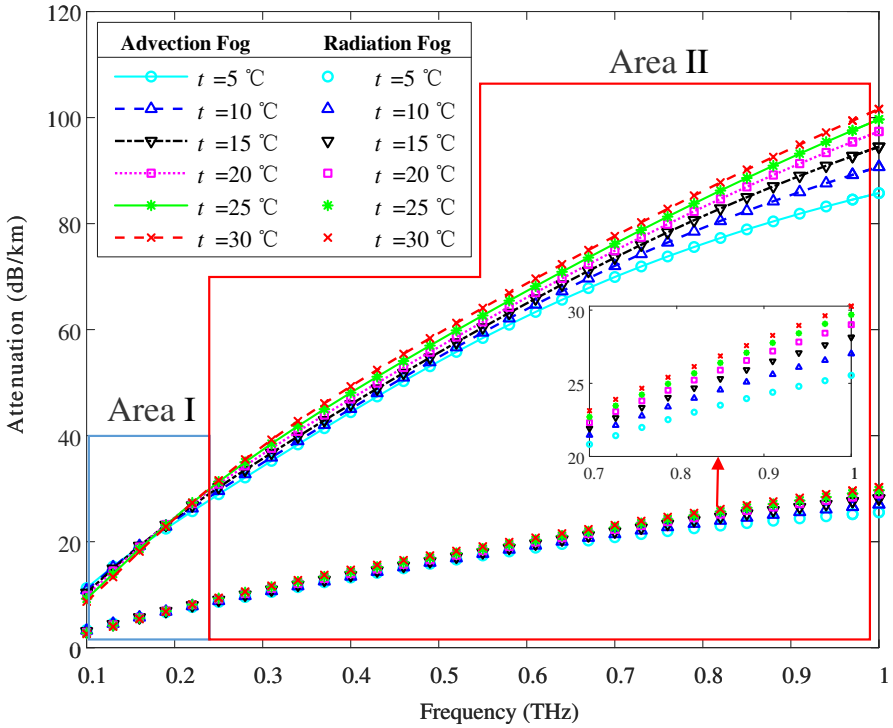

Figure 3. Fog attenuation of terahertz waves at diverse temperatures, where area I is the frequency range of 0.1–0.24 THz, and area II is the range of 0.24–1 THz.

Different water contents in fog under diverse visibility conditions can have an impact on fog attenuation of terahertz waves. Figure 4 illustrates the fog attenuation at a temperature of 10 °C, and the simulation results in [18] are represented by a black line with diamonds. There is a strong agreement between the research results in this study with the simulated results in [18]. As shown in Figure 4, attenuation gradually increases with a decrease in visibility and an increase in frequency, and visibility has a greater influence on attenuation. When visibility decreases from 100 m to 50 m, wave attenuation in 1 THz increases by 8.1 dB/km in radiation fog and 27.5 dB/km in advection fog. When visibility

decreases from 50 m to 30 m, terahertz wave attenuation increases by 24.7 dB/km in radiation fog and 47 dB/km in advection fog. Thus, the upward trend in fog attenuation is evidently larger with a decrease in visibility of the fog. Moreover, advection fog attenuation is greater than radiation fog attenuation due to the relatively high density of liquid water.

4.2. Fog Attenuation Based on Mie Theory

In order to investigate the attenuation of advection fog and radiation fog under various visibilities, detailed simulation parameters are shown in Table 2. Figure 5 illustrates the advection fog attenuation and radiation fog attenuation of terahertz waves. The fog attenuation exponentially increases as the frequency increases and the visibility decreases. Specifically, the attenuation exhibits a slow increase at 0.1–0.7 THz and a rapid increase at 0.7–1 THz. The advection fog attenuation at 1 THz is 8488.33 dB, 1999.12 dB, 255.05 dB, and 26.44 dB corresponds to visibility values of 30 m, 50 m, 100 m, and 200 m, respectively. Overall, advection fog causes significantly higher attenuation of terahertz waves compared with radiation fog, and the rate of increase in advection fog attenuation is more pronounced than that of radiation fog attenuation.

The calculation of fog attenuation through Mie theory involves the extinction efficiency factor and particle distribution. While the results are precise, this model is most appropriate for large-sized particles to characterize the absorption and scattering effects. In comparison, Rayleigh approximation is used to analyze the absorption and scattering effects of small-sized particles in the low-terahertz band. Thus, there is a significant difference between fog attenuation calculated based on these two models. Moreover, radiation fog is characterized by a low water content and relatively small droplet particles. Hence, Mie theory may not be suitable for calculating terahertz wave attenuation in radiation fog. According to the numerical simulation results, in the case of advection fog, relatively accurate results can be obtained by using Rayleigh approximation theory at 0.1–0.8 THz and Mie theory at 0.8–1 THz. In the case of radiation fog, it is recommended to employ Rayleigh approximation theory.

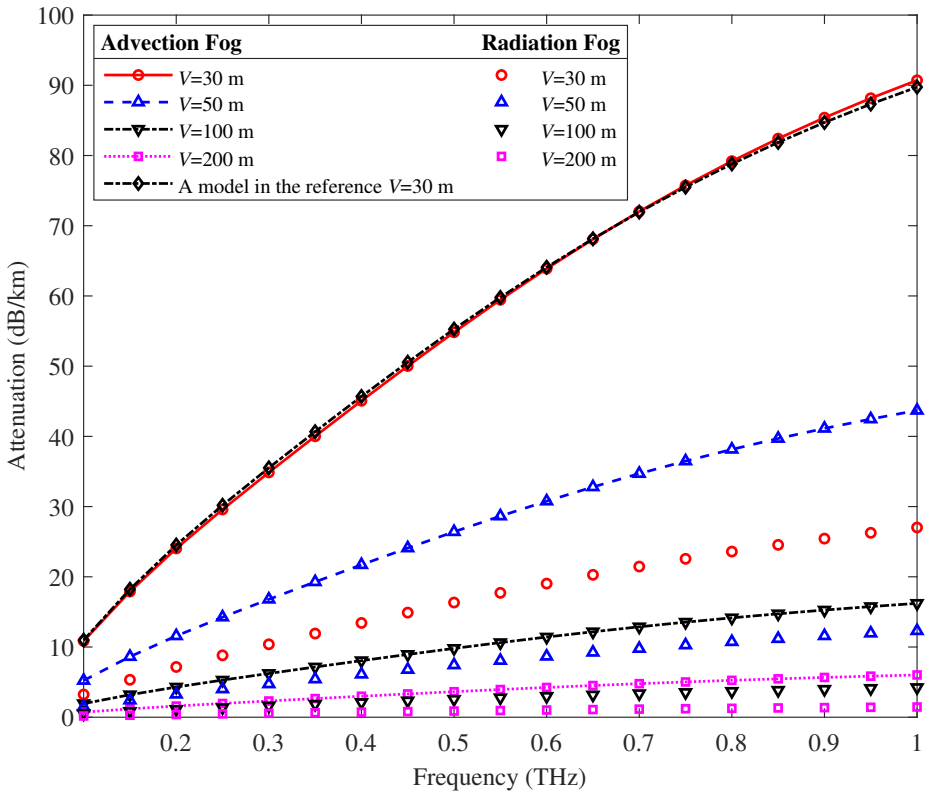

Figure 4. Fog attenuation of THz waves under diverse visibility and comparison with [18].

Table 2. Simulation parameters based on Mie theory.

Parameter	Parameter Values in Fog	Parameter Values in Rain
Particle Radius	1∼60 μm	0.01∼40 mm
Frequency Band	0.1∼1 THz	0.1∼1 THz
Refractive Index	1.5 + 0.01*i*	1.5 + 0.01*i*

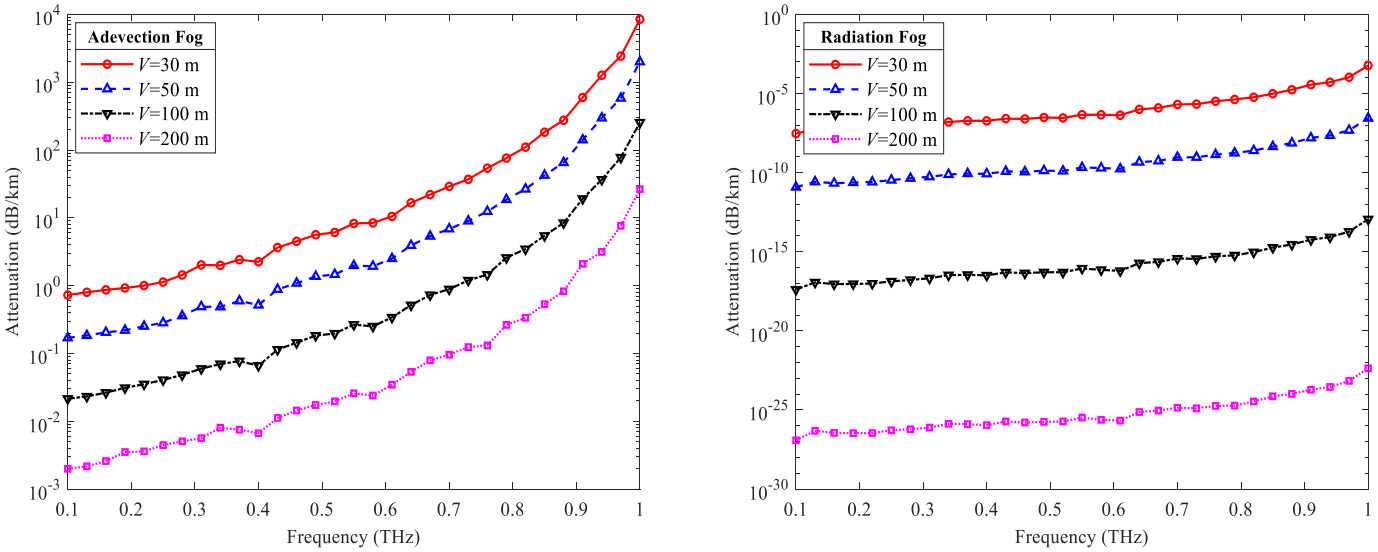

(a) (b)

Figure 5. (**a**) Advection fog attenuation under various visibilities; (**b**) radiation fog attenuation under various visibilities.

4.3. Rain Attenuation Based on Mie Theory

Detailed simulation parameters for exploring rain attenuation are presented in Table 2. Figure 6 depicts rain attenuation of THz waves under diverse rainfall rates and distributions, i.e., Joss distribution, M-P distribution, and Weibull distribution. According to Figure 6, rain attenuation of THz waves is relatively low at 0.1–0.7 THz and high at 0.7–1 THz. The rain attenuation increases exponentially with the increase of both frequency and rainfall rate. For the Joss distribution, the attenuation values at 1 THz are 7757.33 dB, 532.83 dB, 16.59 dB and 2.02 dB. The attenuation values at 1 THz for the M-P distribution are 4718.04 dB, 608.95 dB, 94.05 dB and 16.93 dB. The attenuation values at 1 THz for the Weibull distribution are 4500.98 dB, 411.22 dB, 66.38 dB and 19.32 dB. Meanwhile these four values correspond to the rainfall rate of 2 mm/h, 5 mm/h, 15 mm/h, and 55 mm/h, respectively.

For the Joss distribution, the rainstorms attenuation of terahertz waves is the largest. The drizzle, moderate rain, and downpour attenuations of terahertz waves are smaller than those under the M-P distribution. The terahertz wave attenuation under the Weibull distribution is smaller than that under the M-P distribution for the first three rainfall rates, but the difference is not significant. The downpour and rainstorm attenuation of terahertz waves under the Joss distribution is more significant than that under the Weibull distribution, while drizzle and moderate rain attenuations of terahertz waves are smaller than those under the Weibull distribution. Therefore, different distributions significantly impact the rain attenuation of terahertz waves.

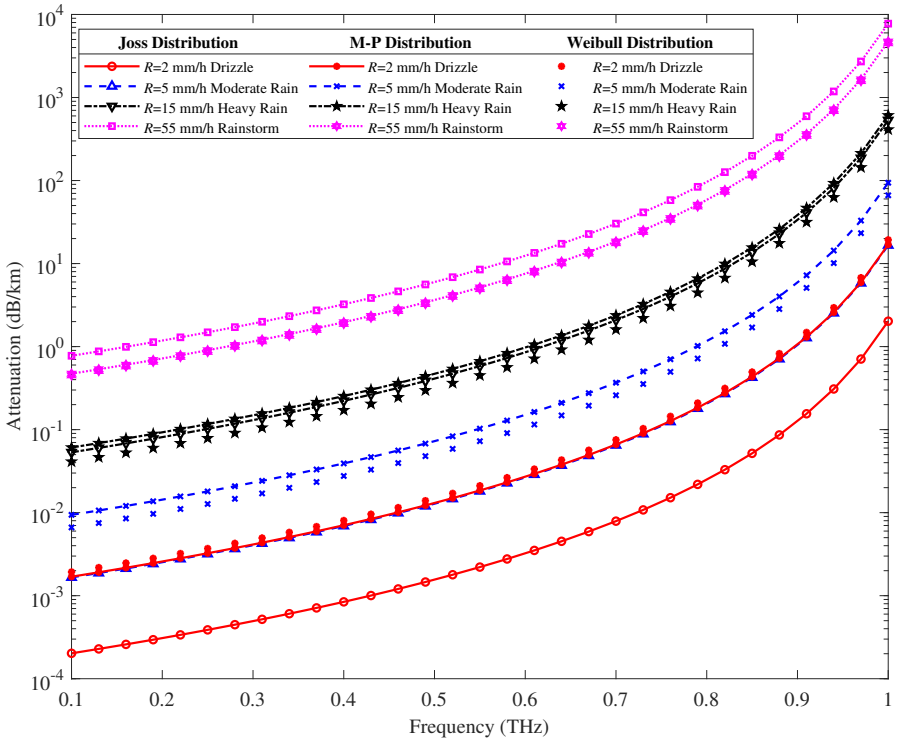

Figure 6. Rain attenuation of THz waves under diverse rainfall rates and distributions.

5. Conclusions

We characterized the attenuation of terahertz waves in foggy and rainy conditions at 0.1–1 THz frequencies using Rayleigh approximation theory and Mie theory. We found that at different temperatures, the influence of temperature on fog attenuation of terahertz waves is greater at high frequencies and smaller at low frequencies. Additionally, a decrease in visibility and an increase in frequency leadsto an exponential increase in fog attenuation, with visibility having a more significant influence than frequency. For advection fog, it is recommended to use Rayleigh approximation theory at 0.1–0.8 THz band and Mie theory at 0.8–1 THz band. On the other hand, for radiation fog, the preferable theory to use is Rayleigh approximation theory. Advection fog attenuation at 1 THz is 8488.33 dB, 1999.12 dB, 255.05 dB, and 26.44 dB, and radiation fog attenuation at 1 THz is 27.02 dB, 12.31 dB, 4.23 dB, and 1.46 dB, corresponding to visibility values of 30 m, 50 m, 100 m, and 200 m, respectively. In addition, the rain attenuation of terahertz waves exponentially increases with frequency and rainfall rate, with significant differences observed among diverse raindrop distributions. The rainfall rate and frequency have a greater impact than raindrop distribution on rain attenuation. For the Joss distribution, the attenuation values at 1 THz are 7757.33 dB, 532.83 dB, 16.59 dB, and 2.02 dB. The attenuation values at 1 THz for the M-P distribution are 4718.04 dB, 608.95 dB, 94.05 dB, and 16.93 dB. The attenuation values at 1 THz for the Weibull distribution are 4500.98 dB, 411.22 dB, 66.38 dB, and 19.32 dB. These four values correspond to rainfall rates of 2 mm/h, 5 mm/h, 15 mm/h, and 55 mm/h, respectively. In the future, actual measurements of terahertz wave attenuation will be conducted in foggy and rainy conditions, which will be beneficial for accurately estimating the path loss and link budget in outdoor environments.

Author Contributions: Conceptualization, X.L.(Xi Liao) and Y.W.; methodology, X.L. (Xi Liao) and L.F.; investigation, X.L. (Xi Liao) and L.F.; resources, Y.W., Z.Y., G.W., X.L. (Xianjin Li) and J.Z.; data curation, L.F.; visualization, X.L. (Xi Liao) and L.F.; writing—original draft preparation, L.F.; writing—review and editing, X.L. (Xi Liao) and L.F.; supervision, X.L. (Xi Liao) and Y.W.; project administration, funding acquisition, X.L. (Xi Liao), Y.W., Z.Y., G.W., X.L. (Xianjin Li) and J.Z. All authors have read and agreed to the published version of the manuscript.

Funding: This work was supported in part by the National Natural Science Foundation of China under grants 62271095 and 62171071, the Natural Science Foundation of Chongqing under grant cstc2021jcyj-msxmX0634, and the Natural Science Foundation Innovation and Development Joint Fund (Municipal Education Commission) project of Chongqing under grant 2022NSCQ-LZX0107.

Data Availability Statement: The data presented in this study are available on request from the corresponding author.

Conflicts of Interest: The authors declare no conflict of interest.

References

1. Rikkinen, K.; Kyosti, P.; Leinonen, M.E.; Berg, M.; Parssinen, A. THz Radio Communication: Link Budget Analysis toward 6G. *IEEE Commun. Mag.* **2020**, *58*, 22–27. [CrossRef]
2. Dang, S.; Amin, O.; Shihada, B.; Alouini, M.S. What should 6G be? *Nat. Electron.* **2020**, *3*, 20–29. [CrossRef]
3. Han, C.; Wang, Y.; Li, Y.; Chen, Y.; Abbasi, N. A.; Kürner, T.; Molisch, A.F. Terahertz Wireless Channels: A Holistic Survey on Measurement, Modeling, and Analysis. *IEEE Commun. Surv. Tutor.* **2022**, *24*, 1670–1707. [CrossRef]
4. Chen, Z.; Ma, X.; Zhang, B.; Zhang, Y.; Niu, Z.; Kuang, N.; Chen, W.; Li, L.; Li, S. A Survey on Terahertz Communications. *China Commun.* **2019**, *16*, 1–35. [CrossRef]
5. Guan, K.; Yi, H.; He, D.; Ai, B.; Zhong, Z. Towards 6G: Paradigm of Realistic Terahertz Channel Modeling. *China Commun.* **2021**, *18*, 1–18. [CrossRef]
6. Mittleman, D.M. Twenty Years of Terahertz Imaging. *Opt. Express.* **2018**, *26*, 9417–9431. [CrossRef] [PubMed]
7. Sengupta, K.; Nagatsuma, T.; Mittleman, D.M. Terahertz Integrated Electronic and Hybrid Electronic-Photonic Systems. *Nat. Electron.* **2018**, *1*, 622–635. [CrossRef]
8. Sarieddeen, H.; Alouini, M. S.; Al-Naffouri, T.Y. An Overview of Signal Processing Techniques for Terahertz Communications. *Proc. IEEE.* **2021**, *109*, 1628–1665. [CrossRef]
9. Headland, D.; Monnai, Y.; Abbott, D.; Fumeaux, C.; Withayachumnankul, W. Tutorial: Terahertz Beamforming, from Concepts to Realizations. *APL Phontonics* **2018**, *3*, 051101. [CrossRef]
10. Chen, H.; Sarieddeen, H.; Ballal, T.; Wymeersch, H.; Alouini, M.S.; Al-Naffouri, T.Y. A Tutorial on Terahertz-Band Localization for 6G Communication Systems. *IEEE Commun. Surv. Tutor.* **2022**, *4*, 1780–1815. [CrossRef]
11. Lemic, F.; Abadal, S.; Tavernier, W.; Stroobant, P.; Colle, D.; Alarcón, E.; Marquez-Barja, J.; Famaey, J. Survey on Terahertz Nanocommunication and Networking: A Top-Down Perspective. *IEEE J. Sel.* **2021**, *39*, 1506–1543. [CrossRef]
12. Ishii, S.; Kinugawa, M.; Wakiyama, S.; Sayama, S.; Kamei, T. Rain Attenuation in the Microwave-to-Terahertz Waveband. *Wireless Eng. Technol.* **2016**, *7*, 59. [CrossRef]
13. Su, K.; Moeller, L.; Barat, R.B.; Federici, J.F. Experimental Comparison of Performance Degradation from Terahertz and Infrared Wireless Links in Fog. *J. Opt. Soc. Am. A-Opt. Image Sci. Vis.* **2012**, *29*, 179–184. [CrossRef] [PubMed]
14. Siles, G.A.; Riera, J.M.; Garcia-del-Pino, P. Atmospheric Attenuation in Wireless Communication Systems at Millimeter and THz Frequencies. *IEEE Antennas Propag. Mag.* **2015**, *57*, 48–61. [CrossRef]
15. Moon, E.B.; Jeon, T.I.; Grischkowsky, D.R. Long-Path THz-TDS Atmospheric Measurements Between Buildings. *IEEE Trans. Terahertz Sci. Technol.* **2015**, *5*, 742–750. [CrossRef]
16. Schneider, T.; Wiatrek, A.; Preußler, S.; Grigat, M.; Braun, R.P. Link Budget Analysis for Terahertz Fixed Wireless Links. *IEEE Trans. Terahertz Sci. Technol.* **2012**, *2*, 250–256. [CrossRef]
17. Jing, Q.; Liu, D.; Tong, J. Study on the Scattering Effect of Terahertz Waves in Near-Surface Atmosphere. *IEEE Access.* **2018**, *6*, 49007–49018. [CrossRef]
18. Haiying, L.; Zhensen, W.; Leke, L.; Zhenwei, Z.; Changsheng, L.; Xin, Z. The Analysis of Advection Fog Attenuation Algorithms in Terahertz Wave Band. In Proceedings of the 2014 XXXIth URSI General Assembly and Scientific Symposium (URSI GASS), Beijing, China, 16–23 August 2014; pp. 1–4. [Crossref]
19. Yang, Y.; Mandehgar, M.; Grischkowsky, D. R. Broadband THz Signals Propagate Through Dense Fog. *IEEE Photonics Technol. Lett.* **2015**, *27*, 383–386. [CrossRef]
20. Golovachev, Y.; Etinger, A.; Pinhasi, G. A.; Pinhasi, Y. Propagation Properties of Sub-Millimeter Waves in Foggy Conditions. *J. Appl. Phys.* **2019**, *125*, 151612. [CrossRef]
21. Al-Baidhani, A.; Fan, H.H. Learning for detection: A deep learning wireless communication receiver over Rayleigh fading channels. In Proceedings of the International Conference on Computing, Networking and Communications (ICNC), Honolulu, HI, USA, 18–21 February 2019; pp. 6–10. [Crossref]
22. Gómez-Déniz, E.; Gómez, L.; Gómez, H. W. The slashed-Rayleigh fading channel distribution. *Math. Probl. Eng.* **2019**, *2019*, 1–14. [CrossRef]
23. Ma, J.; Vorrius, F.; Lamb, L.; Moeller, L.; Federici, J.F. Experimental Comparison of Terahertz and Infrared Signaling in Laboratory-Controlled Rain. *J. Infrared Millim. Terahertz Waves.* **2015**, *36*, 856–865. [CrossRef]
24. Ma, J.; Vorrius, F.; Lamb, L.; Moeller, L.; Federici, J.F. Comparison of Experimental and Theoretical Determined Terahertz Attenuation in Controlled Rain. *J. Infrared Millim. Terahertz Waves* **2015**, *36*, 1195–1202. [CrossRef]

25. Morais, L.; Menezes, L.; Moraes, P. Rain Attenuation at THz Frequencies from Historical Data Collected in Brasilia, Brazil. In Proceedings of the 2021 USNC-URSI Radio Science Meeting (USCN-URSI RSM), Honolulu, HI, USA, 9–13 August 2021; pp. 45–50. [Crossref]
26. Yoseva, M.; Hashiguchi, H.; Vonnisa, M.; Luini, L.; Nugroho, S.; Shafii, M.A. Characteristics of Rain Attenuation for Microwave-to-terahertz Waveband from Raindrop Size Distribution Observation in Indonesia. In Proceedings of the 2019 PhotonIcs and Electromagnetics Research Symposium—Spring (PIERS-Spring), Rome, Italy, 17–20 June 2019; pp. 362–367. [Crossref]
27. Norouzian, F.; Marchetti, E.; Gashinova, M.; Hoare, E.; Constantinou, C.; Gardner, P.; Cherniakov, M. Rain Attenuation at Millimeter Wave and Low-THz Frequencies. *IEEE Trans. Antennas Propag.* **2020**, *68*, 421–431. [CrossRef]
28. Bohren, C. F.; Huffman, D.R. *Absorption and Scattering of Light by Small Particles*; John Wiley and Sons: New York, NY, USA, 2008. Available online: https://www.researchgate.net/publication/200455938_Absorption_and_scattering_of_light_by_small_particles (accessed on 10 February 2022).
29. Xizheng, K.; Dongdong, M.; Jiani, L. Study Attenuation of Laser Transmission in Fog. *J. Light Scat.* **2009**, *21*, 104–109. [Crossref]
30. Joss, J. The Variation of Raindrop Size Distributions at Locarno. *Proc. Int. Conf. Cloud Phys.* **1968**, *1968*, 369–373. Available online: https://cir.nii.ac.jp/crid/1570291226437816064 (accessed on 15 May 2022).
31. Marshall, J. S.; Palmer, W. The Distribution of Raindrops with Size. *J. Meteorol.* **1948**, *5*, 165–166. [CrossRef]
32. Jiang, H.; Sano, M.; Sekine, M. Weibull Raindrop-Size Distribution and Its Application to Rain Attenuation. *IEE Proc. Microwaves Antennas. Propag.* **1997**, *144*, 197–200. [CrossRef]
33. Attenuation Due to Clouds and Fog. Document Rec. ITU-R P. 840-8, 2019, International Telecommunication Union. Available online: https://www.itu.int/rec/R-REC-P.840/en (accessed on 12 November 2021).
34. Mätzler, C. *MATLAB Functions for Mie Scattering and Absorption*; 2nd ed.; Institute of Applied Physics, University of Bern: Bern, Switzerland, 2002. [Crossref]